Special Anniversary Issue: Professor Jan Czochralski Year 2013 — Invited Paper

Czochralski Growth and Optical Properties of $(Lu_xGd_{1-x})_2SiO_5$ Solid Solution Crystals Single Doped with Sm^{3+} and Dy^{3+}

W. Ryba-Romanowski[a,*], A. Strzęp[a], M. Głowacki[b], R. Lisiecki[a], P. Solarz[a] and J.Z. Domagala[b]

[a]Institute of Low Temperature and Structure Research, Polish Academy of Sciences Okólna 2, 50-422 Wrocław, Poland

[b]Institute of Physics, Polish Academy of Sciences, al. Lotników 32/46, 02-668 Warsaw, Poland

Solid solution crystals $(Lu_xGd_{1-x})_2SiO_5$ single doped with Sm^{3+} and Dy^{3+} were grown by the Czochralski method. Segregation coefficients Lu/Gd, melting temperatures and structures of solid solution crystals were determined for $0.15 \leq x \leq 0.8$. It was found that for $x \geq 0.17$ the crystals belong to the monoclinic system within a space group $C2/c$ and their melting temperature diminishes monotonously from 1990 °C to 1780 °C when x decreases from 0.8 to 0.15. Disparity of ionic radii of Lu^{3+} and Gd^{3+} induces structural disorder that brings about an inhomogeneous broadening of spectral lines in absorption and emission spectra of incorporated luminescent Sm^{3+} and Dy^{3+} ions. Optical properties of obtained crystals were determined based on results of measurement of absorption and emission spectra and luminescence decay curves. Spectroscopic investigation revealed that Sm^{3+} doped crystals show intense emission distributed in the visible-near infrared region with the most intense band centred at 605 nm and characterized by a branching ratio of 0.43. Emission spectrum of Dy^{3+} doped crystals is dominated by a band centred at 575 nm and characterized by a branching ratio of 0.58. It has been concluded that the systems under study are potential laser materials able to generate visible emission upon GaN/InGaN laser diode pumping.

DOI: 10.12693/APhysPolA.124.321

PACS: 42.55.Rz, 42.70.Hj, 78.40.−q, 78.55.Fv

1. Introduction

A long-lasting interest in yttrium orthosilicate Y_2SiO_5, gadolinium orthosilicate Gd_2SiO_5, and lutetium orthosilicate Lu_2SiO_5 crystals has been stimulated by a search for reliable hosts offering an ability to incorporate appreciable amounts of rare earth ions and thereby show desired luminescent and laser properties. In early works suitability of Y_2SiO_5:Er^{3+} and Y_2SiO_5:Tm^{3+} systems for the design of infrared lasers has been demonstrated and their laser performance has been determined [1, 2]. Later on an efficient laser operation of Y_2SiO_5:Yb^{3+} and Lu_2SiO_5:Yb^{3+} under high-power diode-pumping has been reported [3]. Recently, an advantage of inhomogeneous line broadening of Yb^{3+} emission in a solid solution crystal Y_2SiO_5–Gd_2SiO_5 (GYSO) has been taken to obtain femtosecond operation of a diode-pumped GYSO:Yb laser [4].

A lot of attention has been paid also during last two decades to cerium-doped orthosilicate crystals in order to explore their potential as scintillating materials. Numerous papers have been devoted to elucidate the scintillation mechanism and to assess the efficiency of scintillation in Gd_2SiO_5:Ce^{3+} [5, 6], Y_2SiO_5:Ce^{3+} [6, 7], Lu_2SiO_5:Ce^{3+} [8] and in cerium-doped solid solution crystals Lu_2SiO_5–Y_2SiO_5 (LYSO) [9]. Accumulated knowledge in this topic made it possible to categorize cerium-doped orthosilicate crystals among the best scintillating materials for practical purposes [9].

In contrast to findings mentioned above the information on potential of rare earth-doped orthosilicate crystals for application as phosphors or laser materials emitting in the visible is poor. In several papers, spectroscopic features of praseodymium-doped Y_2SiO_5 crystals have been investigated aiming at assessment of their application as fast scintillators [10]. Also, phenomenon of quantum cutting in europium-doped Gd_2SiO_5 has been examined to find out whether this system may be promising as VUV-excited visible phosphor [11].

This paper deals with crystal growth, structural peculiarities and spectroscopic features of solid solution Lu_2SiO_5–Gd_2SiO_5 (LGSO) crystals doped with Dy^{3+} and Sm^{3+} ions. The choice of systems for the study is motivated by several reasons.

First, recent progress in the field of blue light emitting diodes and GaN/InGaN lasers opens new ways for optical pumping that can overcome the problem of poor absorption efficiency regarded as main shortcoming of Dy^{3+} and Sm^{3+} ions. In fact, spectroscopic studies of Lu_2SiO_5:Dy^{3+} reported in [12] and of Gd_2SiO_5:Sm^{3+} reported in [13] have revealed that these systems offer intense absorption lines that match emission wavelengths of GaN/InGaN lasers emitting at 390 nm and 405 nm, respectively.

*corresponding author; e-mail: W.Ryba-Romanowski@int.pan.wroc.pl

Second, a luminescent material may be of interest for practice provided that its manufacturing is easy and non expensive. Systems mentioned above do not meet these requirements, however. Gd_2SiO_5 crystal is strongly prone to cleave thereby cutting and polishing is difficult. On the other hand, a high melting temperature combined with a high cost of lutetium oxide put Lu_2SiO_5 host at a disadvantage. These shortcomings can be markedly reduced when growing crystals of solid solutions $(Lu_xGd_{1-x})_2SiO_5$. It has been reported recently [14] that the LGSO crystals retain the crystal structure inherent to Lu_2SiO_5 when $x \geq 0.17$ whereas the melting temperature amounting to 2050 °C for Lu_2SiO_5 diminishes monotonously with decreasing x value and becomes close to 1820 °C for $x = 0.20$. It is expected that owing to significant disparity of ionic radii of Gd^{3+} and Lu^{3+} the crystal structure of LGSO will show a certain degree of structural disorder. As a consequence spectral lines of incorporated rare earth ions would be affected by an inhomogeneous broadening thereby improving the spectral overlap between emission bands of laser diodes and absorption bands available for optical pumping. Intention of the present work is to determine the effect of the substitution of lutetium by gadolinium on peculiarities of crystal growth and on spectroscopic features relevant to luminescence and potential visible laser operation of $(Lu_xGd_{1-x})_2SiO_5$ crystals doped with samarium and dysprosium.

Obtained results will be discussed with reference to papers mentioned above [12–16].

2. Structural considerations

Gd_2SiO_5 forms crystals belonging to the monoclinic system with a space group $P2_1/c$. They are characterized by unit cell parameters $a = 9.139$, $b = 7.075$, $c = 6.852$ Å and $\beta = 107.696°$. This structure is built up from GdO_4 tetrahedra arranged in a two-dimensional network parallel to the (100) plane and SiO_4 tetrahedra located in the wide meshes of this network.

Lu_2SiO_5 forms crystals belonging also to the monoclinic system but within a space group $C2/c$. They are characterized by unit cell parameters $a = 14.271$, $b = 6.646$, $c = 10.261$ Å and $\beta = 122.190°$. This structure contains chains formed by LuO_4 tetrahedra and double Lu_6O_2 tetrahedra arranged along a-axis. The chains are connected by isolated SiO_4 tetrahedra. Figure 1 shows details of first coordination shells of Si^{4+} and RE^{3+} (RE = Gd, Lu) cations in the two systems. In the structure of Gd_2SiO_5, trivalent gadolinium ions are located in two non-equivalent crystallographic sites. One of them is characterized by the coordination number CN = 9 and the site symmetry C_{3v}. Another site has symmetry C_s and CN = 7. In the structure of Lu_2SiO_5 trivalent lutetium ions are located in two non-equivalent sites with the same C_1 symmetry but different CN numbers amounting to 6 and 7. Luminescent rare earth ions incorporated into Gd_2SiO_5 and Lu_2SiO_5 substitute Gd^{3+} and

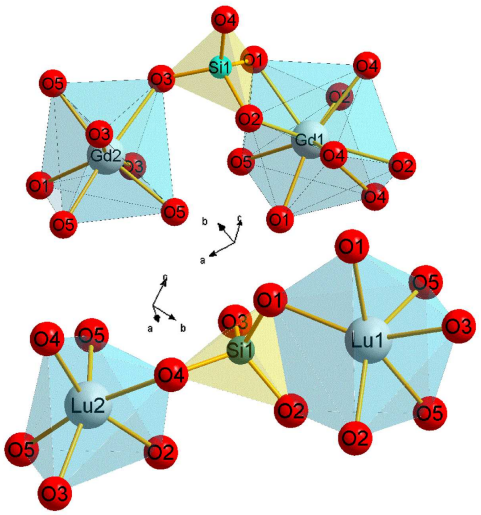

Fig. 1. Nearest coordination shells for cations in the crystal structures of Gd_2SiO_5 (upper) and Lu_2SiO_5 (bottom).

Lu^{3+} ions, respectively and are expected to enter both sites available in these structures. In fact, occurrence of two different Dy^{3+} sites in Lu_2SiO_5 has been evidenced based on low temperature absorption and emission spectra [15].

Systematic structural study has revealed that $(Lu_xGd_{1-x})_2SiO_5$ solid solutions form crystals with the structure inherent to Gd_2SiO_5 when $x < 0.17$ and to Lu_2SiO_5 when $x \geq 0.17$ [14].

3. $(Lu_xGd_{1-x})_2$ SiO_5 single crystal growth

As the initial substances for $(Lu_xGd_{1-x})_2SiO_5$:RE (RE = Sm or Dy) single crystal growth by the Czochralski method were used high purity oxides: Gd_2O_3 (5N purity), Lu_2O_3 (4N) and SiO_2 (4N5), Dy_2O_3 (5N) and Sm_2O_3 (5N). They were dried at $T = 1000$ °C for 4 h, weighted, mixed, formed into pellets and synthesized at 1500 °C for 6 h. Such prepared material was loaded into the 40 mm diameter × 40 mm high iridium crucible. During the growth process the crucible was inductively heated using an RF generator. Orthosilicates crystal growth was performed under nitrogen atmosphere with pulling rate of 1.5–2.5 mm/h and rotation speed of 20 rpm. Ir rod was used as a seed. Crystal diameter was controlled by monitoring the weight of the crucible.

Series of bulk single crystals with various Lu/Gd ratio in crystal matrix doped with Dy or Sm was obtained. Grown crystals were transparent as shown in Fig. 2. Crystals doped with dysprosium were light yellow-greenish, doped with samarium — yellow.

Although all LGSO crystals were grown under similar conditions, the occurrence of defects depended strongly on crystal composition. As it was shown in [14] crystals grown from $(Lu_xGd_{1-x})_2SiO_5$ melt with $x \leq 0.15$

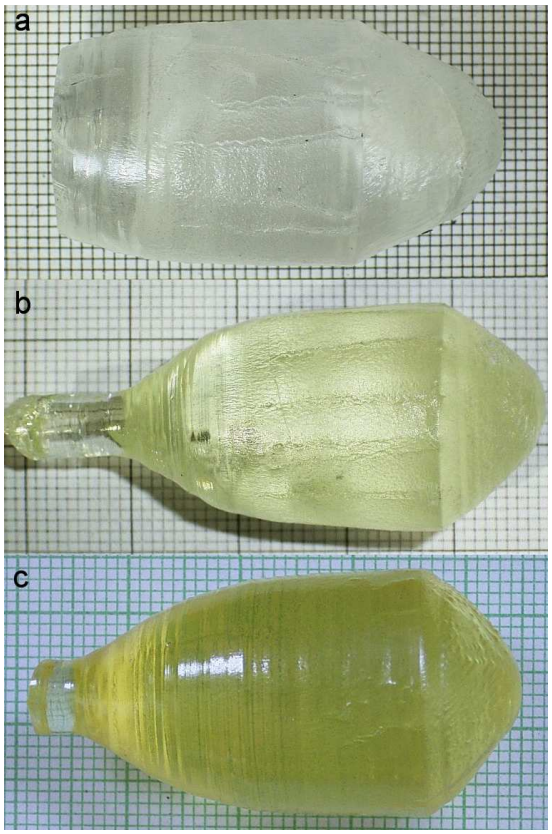

Fig. 2. LGSO single crystals with Lu/Gd ratio = 40/60 ($C2/c$ space group): (a) without dopants, (b) doped with 4 mol.% Dy, (c) doped with 5 mol.% Sm.

crystallize in $P2_1/c$ space group. They show high tendency to crack along (100) plane during cooling, cutting and polishing. Increase of lutetium concentration in the melt to $x = 0.17$ and more results in structural transition to $C2/c$ space group and therefore lack of cleavage plane. Crystals with $x \geq 0.17$ cracked only during cooling near the Ir rod seed due to the different coefficient of thermal expansion of iridium and LGSO. The lowest melting point among investigated crystals was observed for 15/85 Lu/Gd ratio ($P2_1/c$) and 17/83 Lu/Gd ratio ($C2/c$) (1780 °C and 1785 °C, respectively). Chemical composition of these two crystals is close to one causing structural change from $P2_1/c$ to $C2/c$ and that was the cause of numerous defects and cracks. Much better quality with very few defects visible to the naked eye showed crystals with Lu/Gd ratio equal or higher than 20/80. Estimated melting points, chemical compositions of crystals and segregation coefficients are shown in Table.

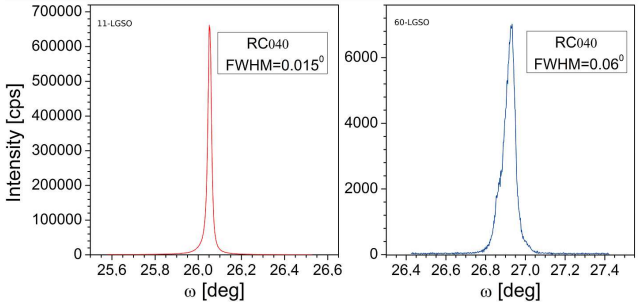

Fig. 3. The X-ray rocking curves for the symmetrical 040 reflections for the two samples — one with $P2_1/c$ structure (11/89 Lu/Gd ratio) — left picture and one with $C2/c$ structure (60/40 Lu/Gd ratio) — right picture.

In order to determine crystal quality high resolution X-ray diffraction measurements were performed. The instrument (Philips X'Pert MRD diffractometer employing the Cu K_{α_1} radiation) was equipped with a four-crystal Ge 220 monochromator and a two-reflection analyser. The X-ray rocking curves are presented in Fig. 3 for the symmetrical 040 reflections for the two samples — one with $P2_1/c$ structure (with 11/89 Lu/Gd ratio) and one with $C2/c$ structure (60/40 Lu/Gd ratio). They indicate a very good crystallographic quality of sample with 11/89 Lu/Gd ratio — full width at half maximum (FWHM) = 0.015°, and less perfect, but still good quality of sample with 60/40 Lu/Gd ratio (FWHM = 0.06°).

TABLE

Chemical composition LGSO crystals measured by TCP–MS method together with nominal composition of melts which crystals were obtained from segregation coefficients and estimated melting points.

Sample	Composition of LGSO:Sm or Dy		Segregation coefficient		Melting point [°C]
	Melt	Crystal	$k_{\text{eff Gd/Lu}}$	$k_{\text{eff Lu/Gd}}$	
80(Lu)–20(Gd)	$(Lu_{0.768}Gd_{0.192}Dy_{0.04})_2SiO_5$	$(Lu_{0.799}Gd_{0.163}Dy_{0.038})_2SiO_5$	0.82	1.22	1990
60(Lu)–40(Gd)	$(Lu_{0.576}Gd_{0.384}Dy_{0.04})_2SiO_5$	$(Lu_{0.634}Gd_{0.331}Dy_{0.035})_2SiO_5$	0.78	1.28	1930
50(Lu)–50(Gd)	$(Lu_{0.500}Gd_{0.495}Sm_{0.005})_2SiO_5$	$(Lu_{0.510}Gd_{0.416}Sm_{0.005})_2SiO_5$	0.82	1.22	1900
40(Lu)–60(Gd)	$(Lu_{0.384}Gd_{0.576}Dy_{0.04})_2SiO_5$	$(Lu_{0.437}Gd_{0.534}Dy_{0.029})_2SiO_5$	0.82	1.22	1870
20(Lu)–80(Gd)	$(Lu_{0.192}Gd_{0.768}Dy_{0.04})_2SiO_5$	$(Lu_{0.220}Gd_{0.740}Dy_{0.039})_2SiO_5$	0.84	1.19	1810
17(Lu)–83(Gd)	$(Lu_{0.170}Gd_{0.825}Sm_{0.005})_2SiO_5$	$(Lu_{0.173}Gd_{0.814}Sm_{0.006})_2SiO_5$	0.97	1.03	1785
15(Lu)–85(Gd)	$(Lu_{0.150}Gd_{0.845}Sm_{0.005})_2SiO_5$	$(Lu_{0.130}Gd_{0.769}Sm_{0.009})_2SiO_5$	1.05	0.95	1780

The observed differences between the results for the two samples occur most likely due to interplanar distance, $d(010)$, spread in 60/40 crystal, which can be possible while almost half of Lu matrix ions is replaced by gadolinium ions. However, an ultimate quantitative assessment of high optical quality of the crystals in terms of loss coefficient can be obtained during planned measurement of their laser performance.

4. Spectroscopic properties

When interpreting experimental results we will refer to energy level diagrams for Sm^{3+} and Dy^{3+} ions shown in Fig. 4. It can be seen that there is a striking similarity between two diagrams in that they consist of one

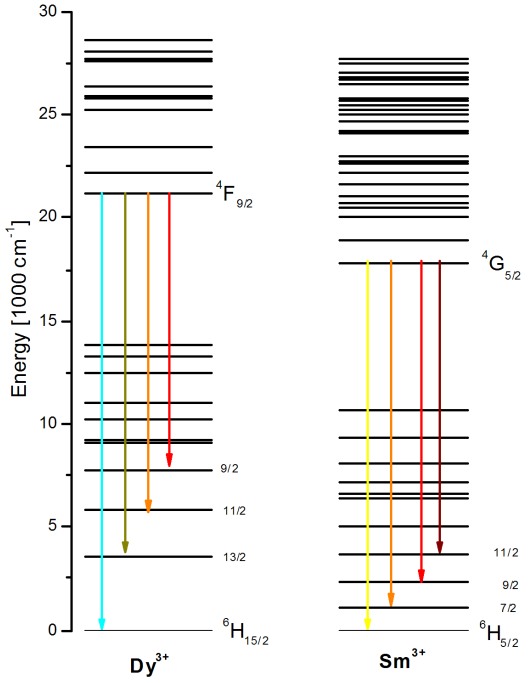

Fig. 4. Energy levels schemes of Sm^{3+} and Dy^{3+} ions. Arrows indicate observed luminescent transitions.

group of relatively closely spaced multiplets formed by a spin–orbit splitting of low energy ^6H and ^6F sextet terms and a second group encompassing high energy multiplets derived from the ^4F, ^4G, ^4H, ^4I, ^4K, ^4L, ^4M quartets and ^6P sextet terms. Although the $4f^5$ electronic configuration of Sm^{3+} and the $4f^9$ electronic configuration of Dy^{3+} are different, the same multiplets appear in energy level diagrams in agreement with Hund's rules.

Two groups of multiplets mentioned above are separated by relatively large energy gaps amounting to 7500 cm^{-1} and 7000 cm^{-1} for Sm^{3+} and Dy^{3+}, respectively. Energy difference between excited levels of rare earth ions is a governing factor that determines competition of radiative and nonradiative processes contributing to decay of energy created by optical absorption. So called "energy gap law" states that the rate W_{mph} of nonradiative multiphonon relaxation of an excited level increases with decreasing energy separation ΔE between an excited level in question and next lower energy level according to the relation $W_{\mathrm{mph}} = C\exp(-\alpha\Delta E)$, where C and α are parameters dependent on the host. As a consequence, solely the $^4G_{5/2}$ level of Sm^{3+} and the $^4F_{9/2}$ level of Dy^{3+} ions in the orthosilicate crystals are metastable and decay by radiative transitions indicated by arrows in Fig. 4.

4.1. Intensities of absorption transitions relevant to optical pumping

In principle, occurrence of numerous excited multiplets above metastable levels of Sm^{3+} and Dy^{3+} is advantageous to optical pumping, especially when using sources that provide a broad-band emission. Unfortunately, optical absorption in this spectral region involving spin-forbidden absorption transitions from the ground sextet state to quartet states is very weak. Figure 5 compares survey absorption spectra recorded at room temperature in the 350–450 nm region for Sm^{3+} and Dy^{3+} ions in $(Lu_xGd_{1-x})_2SiO_5$ crystals differing in x values. Absorption intensities in these spectra are calibrated in units of absorption coefficient α (left vertical axis) and in units of absorption cross section $\sigma = \alpha/N$, where N is rare-earth ions concentration (right vertical axis).

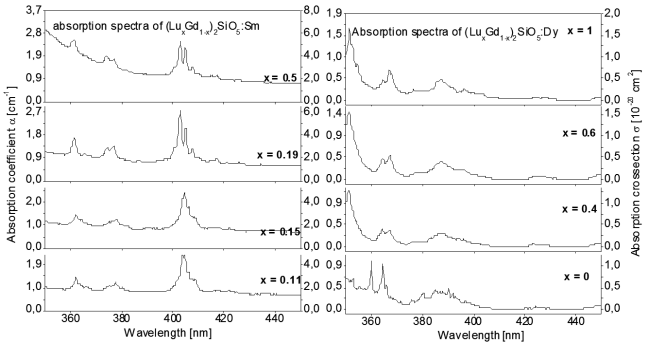

Fig. 5. Survey absorption spectra in UV-visible of $(Lu_xGd_{1-x})_2SiO_5$:Re^{3+} (Re = Dy, Sm), recorded at 300 K for different x values.

The assignment of absorption spectra shown in Fig. 5 is not a trivial task because of weak band intensities combined with small energy separation between excited multiplets involved. However, a general interpretation of absorption band intensities may be proposed based on the Judd–Ofelt theory that relates transition intensities to matrix elements of unit tensor operators $U(t) = (\psi J\|U^t\|\psi' J')^2$ $(t = 2, 4, 6)$ between initial ψJ and terminal $\psi' J'$ levels of the transition. In fact, weak absorption bands in the visible above about 430 nm for Sm^{3+} doped crystal are consistent with extremely small $U(t)$ values calculated in [17] for corresponding transitions between ground sextet and final quartet states. The same applies to Sm^{3+} absorption bands located in the 350–395 nm spectral region. There is however quite

intense Sm^{3+} absorption around 405 related to transitions ending on the $^4M_{19/2}$, $^4L_{13/2}$, $^4P_{5/2}$, $^4F_{7/2}$, $^6P_{5/2}$, and $^6P_{3/2}$ closely spaced multiplets. Numerous transitions contribute to this absorption but its intensity is governed by spin allowed transitions to $^6P_{5/2}$ and $^6P_{3/2}$ sextet states with large U(4) values [17].

Absorption spectra of Dy^{3+} ions in $(Lu_xGd_{1-x})_2SiO_5$ crystals consist of several weak bands located in the visible region between 500 nm and 370 nm and of much more intense and narrow lines in UV region below 370 nm. Absorption lines in the UV region cannot be considered for optical pumping because commercial laser diodes emitting in this spectral region are not yet available. Fortunately, a broad absorption band stretching from about 405 nm to 370 nm is more favourable for this purpose. Spin forbidden transitions from the ground $^6H_{15/2}$ multiplet to the $^4I_{13/2}$, $^4F_{7/2}$, $^4M_{21/2}$, and $^4K_{17/2}$ quartet states contribute to the band intensity since in contrast to Sm^{3+} the excited sextet states of Dy^{3+} ions have higher energy. However, values of $U(t)$ matrix elements between sextet and quartet states for Dy^{3+} ions are markedly larger than those for Sm^{3+} ions [17]. As a consequence, resulting absorption intensity is high enough to be considered for optical pumping.

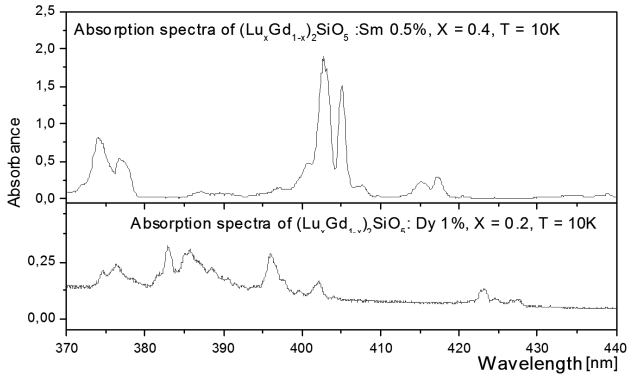

Fig. 6. Details of potential pump bands of Sm^{3+} and Dy^{3+} in $(Lu_xGd_{1-x})_2SiO_5$ crystals recorded at 10 K.

Figure 6 compares details of potential pump bands of Sm^{3+} and Dy^{3+} in $(Lu_xGd_{1-x})_2SiO_5$ crystals recorded at 10 K. Although at 10 K higher energy crystal field levels of the ground state are not populated and absorption transitions originate mainly from the lowest one, the spectra shown consist of poorly resolved and broad band components. This is due to the inhomogeneous line broadening effect combined with spectral overlapping of transitions to numerous closely spaced terminal levels.

$(Lu_xGd_{1-x})_2SiO_5$ are optically biaxial crystals hence absorption intensities of accommodated Sm^{3+} and Dy^{3+} ions are expected to be anisotropic. Anisotropy of pump band should be accounted for when determining an optimal coupling between pump source and luminescent material. Commonly, the importance of the optical anisotropy is assessed based on examination of optical spectra recorded with polarized light. Figure 7 shows polarized pump bands of Sm^{3+} and Dy^{3+} in $(Lu_xGd_{1-x})_2SiO_5$ crystals recorded with the electric vector E of incident light parallel to b crystallographic axis and to x and y optical axes of the crystal. It can be seen in this figure that the anisotropy of the band shapes and intensities of Sm^{3+} absorption is quite large. In particular, peak value of absorption cross-section of the pump band at 405 nm for polarization $E \parallel b$ amounts to 7×10^{-20} cm^2, a value nearly three times higher than that for $E \parallel y$ polarization and twice higher than that for $E \parallel x$ polarization. Anisotropy of potential pump band of Dy^{3+} in the region 370–405 nm is rather weak, however.

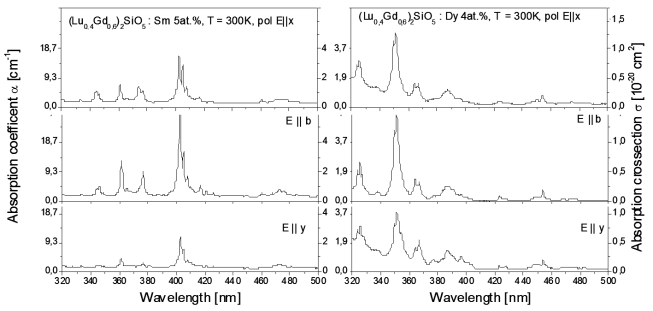

Fig. 7. Room temperature polarized pump bands of Sm^{3+} and Dy^{3+} in $(Lu_xGd_{1-x})_2SiO_5$ crystals recorded with the electric vector E of incident light parallel to b crystallographic axis and to x and y optical axes of the crystal.

4.2. Spectral characteristics of the visible emission

Figure 8 compares survey unpolarized emission spectra recorded at room temperature for Gd_2SiO_5 (upper) and $(Lu_xGd_{1-x})_2SiO_5$ crystals (lower) doped with Sm^{3+} (left) and Dy^{3+} (right). Emission spectrum of Sm^{3+} consists of four bands centered at 565 nm (green band), 605 nm (yellow band), 655 nm (red band) and 720 nm (infrared band), related to transitions from the $^4G_{5/2}$ multiplet to terminal $^6H_{5/2}$, $^6H_{9/2}$, $^6H_{11/2}$, and $^6H_{13/2}$ multiplets, respectively. It can be seen in Fig. 4 that the energy level scheme for Sm^{3+} ions contains several potential terminal levels at higher energy. However, intensities of corresponding infrared transitions are negligibly weak consistently with very small values of $U(t)$ matrix elements involved. Distribution of emission intensity over spectral bands related to transitions ending on different multiplets is commonly expressed in terms of emission branching ratios defined as $\beta_{ij} = \frac{A_{ij}}{\sum_j A_{ij}}$ where A denotes a rate of the transition whereas subscript i denotes the initial multiplet and j denotes possible terminal multiplets. Experimental values of β_{ij} can be determined by numerical integration of bands appearing in the emission spectrum. Following this approach and neglecting infrared transitions ending on terminal multiplets above the $^6H_{13/2}$ the β values were evaluated for Sm^{3+} spectra

shown in Fig. 8. It has been found that the branching ratios β amounting to 0.1142, 0.4347, 0.3569, and 0.0942, for the green, yellow, red, and infrared bands, respectively, are nearly the same when stoichiometry of the host crystal corresponds to $x \geq 0.19$. The approach described above was adopted to assess quantitatively the distribution of emission intensity of Dy^{3+}. It can be seen in Fig. 8 that the Dy^{3+} emission spectrum consists of four bands centered at 485 nm (blue band), 575 nm (yellow band), 665 nm (red band) and at 760 nm (infrared band). All of them are related to transitions from a single metastable level $^4F_{9/2}$. Main dissimilarity between emission spectra of Dy^{3+} and of Sm^{3+} discussed above resides in spectral positions of bands related to transitions terminating in ground states as a consequence of different energy of respective metastable levels.

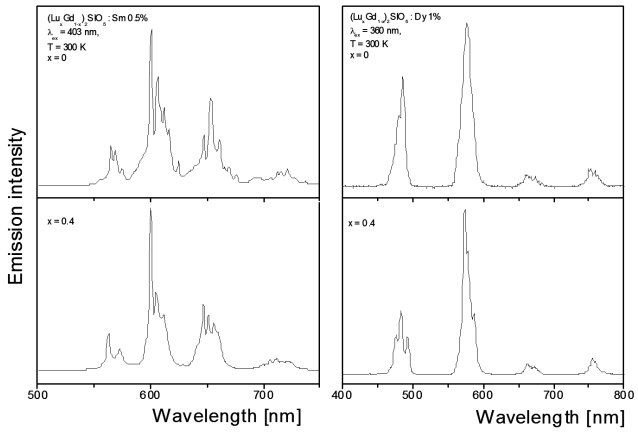

Fig. 8. Survey unpolarized emission spectra recorded at room temperature for $(Lu_xGd_{1-x})_2SiO_5$ crystals doped with Sm^{3+} (left) and Dy^{3+} (right).

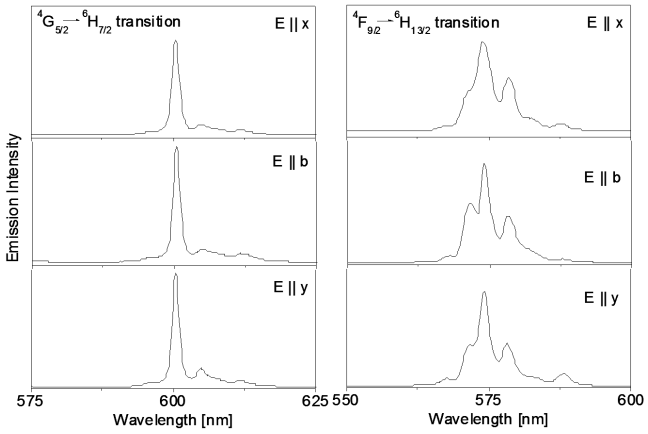

Fig. 9. Details of yellow emission bands related to the $^4G_{5/2}$–$^6H_{7/2}$ transition of Sm^{3+} (left) and to the $^4F_{9/2}$–$^6H_{13/2}$ transition of Dy^{3+} ions (right) in $(Lu_{0.4}Gd_{0.6})_2SiO_5$ host recorded at room temperature with polarized light.

It is worth noticing here that spectral positions of yellow, red, and infrared bands for the two ions do not differ markedly. Experimental values of branching ratios β for Dy^{3+} emission were evaluated by numerical integration of four bands in the spectrum shown in Fig. 8 neglecting marginal contribution of transitions to terminal levels above the $^6F_{11/2}$ level. Evaluated β values are nearly the same when stoichiometry of the host crystal corresponds to $x \geq 0.19$ and equal to 0.2579, 0.5849, 0.0698, and 0.0874, for the blue, yellow, red, and infrared bands, respectively. In the following we will restrict our attention to yellow bands that dominate emission spectra of both the Sm^{3+} and Dy^{3+} doped crystals. When excited levels, which are connected to ground states by fast nonradiative relaxations, are terminal states of transitions, a potential for a low threshold four-level laser operation can be considered. Figure 9 shows details of yellow emission bands related to the $^4G_{5/2}$–$^6H_{7/2}$ transition of Sm^{3+} and to the $^4F_{9/2}$–$^6H_{13/2}$ transition of Dy^{3+} ions in $(Lu_{0.4}Gd_{0.6})_2SiO_5$ host recorded at room temperature with polarized light. In contrast to absorption spectra the anisotropy of Sm^{3+} emission band is rather weak. Slightly more significant anisotropy can be seen in the emission band of Dy^{3+}.

4.3. Excited state relaxation dynamics

Knowledge of processes governing relaxation of excited states is crucial when assessing luminescence efficiency and possibly laser potential of a luminescent material. Flow of energy accumulated in rare earth doped crystals during optical pumping is determined by competing radiative transitions, nonradiative multiphonon relaxation and nonradiative energy transfer between interacting rare earth ions. Fast energy flow from pump levels to metastable levels via nonradiative relaxation followed by mainly radiative decay of the metastable level is highly desired.

Analysis of luminescence decay curves acquired upon short pulse excitation provides useful information regarding relaxation processes of metastable levels. In particular, importance of nonradiative energy transfer may be inferred from comparison of decay curves recorded for samples differing in concentration of rare earth ions. When processes of interaction between rare earth ions are negligible, the lifetime values derived from decay curves result from a competition between radiative decay and multiphonon relaxation. Importance of the latter process may be assessed roughly based on the "energy gap law" mentioned before.

Figure 10 compares semilog plots of luminescence decay curves recorded at room temperature for $(Lu_{0.4}Gd_{0.6})_2SiO_5$ crystals with different concentrations of Sm^{3+} or Dy^{3+} ions. Luminescence decays consistent with a single exponential time dependence for lower activator concentrations become considerably faster and non-exponential when crystals are more heavily doped. It follows from these findings that an adverse "self-quenching" effect is significant for doping levels around several per-

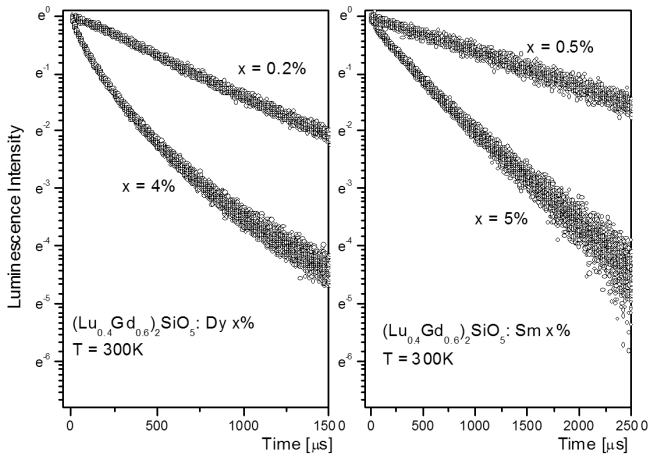

Fig. 10. Semilog plots of luminescence decay curves recorded at room temperature for $(Lu_{0.4}Gd_{0.6})_2SiO_5$ crystals with different concentrations of Sm^{3+} or Dy^{3+} ions.

cent. Lifetime values of 1.8 ms for the $^4G_{5/2}$ level of Sm^{3+} and 0.5 ms for the $^4F_{9/2}$ level of Dy^{3+} follow from single exponential decay curves presented in Fig. 10.

5. Discussion

Fundamental practical advantage of solid solution crystals $(Lu_xGd_{1-x})_2SiO_5$ is that their melting temperature decreases markedly with decreasing x value while retaining the crystal structure inherent to Lu_2SiO_5 for $x \geq 0.17$. When lowering the Lu/Gd ratio in the melt the Czochralski growth of high quality crystals becomes thereby easier and less expensive. Trivalent samarium and dysprosium ions incorporated in $(Lu_xGd_{1-x})_2SiO_5$ crystal host for $0.17 < x < 1$ may reside in two non-equivalent sites with the same C_1 symmetry but differing in the coordination number. However, in contrast to Lu_2SiO_5 ($x = 1$) and to Gd_2SiO_5 ($x = 0$) hosts the nature of Sm^{3+} and Dy^{3+} sites in solid solution crystals may be affected by disparity in radii of cations. In fact, in sixfold-coordinated sites ionic radii of Gd^{3+} and Lu^{3+} ions amount to 0.94 Å and 0.85 Å whereas those for Sm^{3+} and Dy^{3+} ions amount to 0.96 Å and 0.91 Å, respectively [18]. Ionic radii of rare earth ions in sevenfold-coordinated sites are considerably higher, e.g. 1.04 Å for Gd^{3+}. For each particular coordination number ionic radius of Lu^{3+} is inevitably smaller than that of Gd^{3+}. One may thus expect that during growth of $(Lu_xGd_{1-x})_2SiO_5$ crystals bigger ions, i.e. Gd^{3+}, Sm^{3+} and Dy^{3+} will be preferentially retained in the melt.

Data gathered in Table indicate that this is really the case that segregation coefficient Lu/Gd is markedly greater than unity and estimated concentrations of Sm^{3+} and Dy^{3+} in crystals are smaller than intentional. Another consequence of substitution of smaller Lu^{3+} ions by bigger Gd^{3+} ions in solid solution crystals is certain structural disorder that brings about a perturbation of crystal field in sites occupied by luminescent Sm^{3+} and Dy^{3+} ions. Spectroscopic results gathered indicate that the structural disorder induces an inhomogeneous broadening of spectral lines in absorption and emission spectra but does not affect radiative transition intensities. Effect of inhomogeneous broadening of spectral lines is especially favourable when the optical pumping of Sm^{3+}-doped crystals is considered. Intensity of absorption band around 405 nm is advantageously high and ensures sufficient pumping efficiency for Sm^{3+} concentration as low as 0.5%. However, its small bandwidth of several nanometers is comparable to that of laser diode emission. Accordingly, stringent control of a laser diode temperature would be necessary to prevent the degradation of pumping efficiency resulting from the temperature-induced drift of a laser diode emission wavelength. In contrast to Sm^{3+} the bandwidth of Dy^{3+} pump band in the region 370–405 nm is advantageously large but the band intensity is small. In principle, absorption coefficient of the pump band can be increased by the increase of Dy^{3+} concentration. However, when increasing the Dy^{3+} concentration the luminescence intensity decreases due to an adverse self-quenching effect. To determine an optimal Dy^{3+} concentration a trade off between these opposing effects should be carefully considered.

6. Conclusions

Melting temperature of $(Lu_xGd_{1-x})_2SiO_5$ solid solution crystals diminishes monotonously with decreasing x value from about 2050°C for $x = 1$ to 1780°C for $x = 0.15$. When $x \geq 0.17$ the solid solutions form crystals within a space group $C2/c$, inherent to Lu_2SiO_5. Owing to disparity of cationic radii between Gd^{3+} and Lu^{3+} the segregation coefficient Lu/Gd is markedly higher than unity and crystals grown show a certain structural disorder.

Incorporated Sm^{3+} and Dy^{3+} ions reside in two non-equivalent sites with C_1 local symmetry slightly disturbed by structural disorder that brings about an inhomogeneous broadening of spectral lines in absorption and emission spectra but affects weakly transition intensities. Absorption cross-section for potential pump band of Sm^{3+} around 405 nm is advantageously high and ensures efficient absorption efficiency for Sm^{3+} concentration as low as 0.5%. Absorption cross-section for potential pump band of Dy^{3+} located between 370 nm and 405 nm is considerably lower. Both the Sm^{3+} and Dy^{3+} ions in solid solution crystals show intense yellow emission bands thus offering a potential of four level laser operation.

Acknowledgments

This work was supported by National Scientific Committee within a project DEC 2011/01/B/ST7/06166.

References

[1] J.C. Souriau, R. Romero, C. Borel, Ch. Wyon, C. Li, R. Moncorge, *J. Phys. (France)* **4**, C4-373 (1994).

[2] R. Moncorge, H. Manaa, M. Koselia, C. Boulon, C. Madej, J.C. Souriau, C. Borel, Ch. Wyon, *J. Phys. (France)* **4**, C4-377 (1994).

[3] M. Jacquemet, C. Jacquemet, N. Janel, F. Druon, F. Balembois, P. Georges, J. Petit, B. Viana, D. Vivien, B. Ferrand, *Appl. Phys. B* **80**, 171 (2005).

[4] J.F. Zhu, W.L. Tian, J.L. Wang, Z.H. Wang, Z.Y. Wei, L.H. Zheng, L.B. Su, J. Xu, *Opt. Lett.* **17**, 5190 (2012).

[5] K. Takagi, T. Fukazawa, *Appl. Phys. Lett.* **42**, 43 (1983).

[6] H. Loudyi, Y. Guyot, J.-C. Gacon, C. Pedrini, M.-F. Joubert, *Opt. Mater.* **30**, 26 (2007).

[7] W. Drozdowski, A.J. Wójtowicz, D. Wisniewski, P. Szupryczyński, S. Janus, J.-L. Lefaucheur, Z. Gou, *J. Alloys Comp.* **380**, 146 (2004).

[8] B. Liu, C. Shi, M. Yin, Y. Fu, G. Zhang, G. Ren, *J. Lumin.* **117**, 129 (2006).

[9] J. Chen, L. Zhang, R.-Y. Zhu, *Nucl. Instr. Methods Phys. Res. A* **572**, 218 (2007).

[10] A. Novoselov, H. Ogino, A. Yoshikawa, M. Nikl, J. Pejchal, A. Breitlerova, T. Fukuda, *Opt. Mater.* **29**, 1381 (2007).

[11] Y. Chen, B. Liu, C. Shi, M. Kirm, M. True, S. Vielhauer, G. Zimmerer, *J. Phys., Condens. Matter* **17**, 1217 (2005).

[12] R. Lisiecki, G. Dominiak-Dzik, P. Solarz, W. Ryba-Romanowski, M. Berkowski, M. Głowacki, *Appl. Phys. B* **98**, 337 (2010).

[13] A. Strzęp, R. Lisiecki, P. Solarz, G. Dominiak-Dzik, W. Ryba-Romanowski, M. Berkowski, *Appl. Phys. B* **106**, 85 (2012).

[14] M. Głowacki, G. Dominiak-Dzik, W. Ryba-Romanowski, R. Lisiecki, A. Strzęp, T. Runka, M. Drozdowski, V. Domukhovski, R. Diduszko, M. Berkowski, *J. Solid State Chem.* **186**, 268 (2012).

[15] G. Dominiak-Dzik, W. Ryba-Romanowski, R. Lisiecki, P. Solarz, M. Berkowski, *Appl. Phys. B* **99**, 285 (2010).

[16] G. Dominiak-Dzik, W. Ryba-Romanowski, R. Lisiecki, P. Solarz, B. Macalik, M. Berkowski, M. Głowacki, V. Domukhovski, *Crystal Growth Design* **10**, 3522 (2010).

[17] W.T. Carnall, F.R. Fields, K. Rajnak, *J. Chem. Phys.* **49**, 4424 (1968).

[18] R.D. Shannon, C.T. Prewitt, *Acta Crystallogr. B* **25**, 925 (1969).